JOURNAL OF SOLID STATE CHEMISTRY **123,** 398–407 (1996)
ARTICLE NO. 0195

Photoluminescence of Ce^{3+}, Tb^{3+}, and Mn^{2+} in Glasses of Base Composition $LaMgB_5O_{10}$

N. El Jouhari, C. Parent, and G. Le Flem

Institut de Chimie de la Matière Condensée de Bordeaux, Château Brivazac, Avenue du Dr. A. Schweitzer, 33608 Pessac Cédex, France

Received October 23, 1995; in revised form February 2, 1996; accepted March 4, 1996

The photoluminescence of Ce^{3+}, Tb^{3+}, and Mn^{2+} ions was studied in glasses of base composition $LaMgB_5O_{10}$. An NMR spectroscopy investigation proved the close arrangement of the boron oxygen network in both crystalline and vitreous phases. Ce^{3+} occupies two families of sites and acts in codoped glasses as a donor in the processes of the Tb^{3+} and Mn^{2+} luminescences. A detailed analysis of the $Ce^{3+} \rightarrow Mn^{2+}$ energy transfer evidences the increasing influence of the exchange mechanism as the Mn^{2+} acceptor concentration increases. Finally the combined luminescences of the three activators under a unique UV excitation allows the observation of white light.

I. INTRODUCTION

Recently white light generation by vitreous materials was reported for the first time (1). It was obtained from the simultaneous emission of blue, green, and red emitting centers under a unique UV excitation. These materials are borate-based glasses with alkali and alkali-earth as modifiers and contain Ce^{3+}, Tb^{3+}, and Mn^{2+} as activators. Ce^{3+} exhibits a broad band emission centred at the border between the UV and visible ranges. In codoped glasses, this ion acts also as a sensitizer transferring a part of its energy to Tb^{3+} and Mn^{2+}.

On the other hand, in the context of research of new phosphors for luminescent devices, e.g., fluorescent lamps, crystallized borates of composition $LnMgB_5O_{10}$ (Ln = Rare Earth) activated with cerium and manganese (2) or cerium, terbium, and manganese (3) have been shown to give efficient green, red, or white emitting phosphors.

Therefore it was attractive to study glasses of almost identical composition to compare the respective performances of both crystalline and glassy materials. The detailed analysis of the luminescent properties of such materials required the investigation of the energy transfer mechanism between Ce^{3+} and Mn^{2+} in the case of codoped glasses.

In this paper, Section II describes the elaboration of glasses as well as the experimental procedure for the spectroscopic measurements. Section III is devoted to a structural analysis using boron-NMR spectroscopy and to a characterization by magnetic measurements. Section IV examines the luminescence properties of single activated glasses respectively by Ce^{3+}, Tb^{3+}, and Mn^{2+}. Section V discusses the mechanism of the $Ce^{3+} \rightarrow Mn^{2+}$ energy transfer. Last, Section VI describes the luminescence of glasses simultaneously activated by Ce^{3+}, Tb^{3+}, and Mn^{2+} from the point of view of white light generation.

II. EXPERIMENTAL PROCEDURE

II.1. Materials

The investigated glasses had the nominal composition $(11.5\text{-}x\text{-}y)La_2O_3$–$xCe_2O_3$–$yTb_2O_3$–$1As_2O_3$–$(25\text{-}z)MgO$–$z$ MnO–$62.5B_2O_3$, with $0 \leq x \leq 11.5$, $0 \leq y \leq 11.5$, and $0 \leq z \leq 25$. As_2O_3 was introduced to prevent oxidation of Ce^{3+}, Tb^{3+}, and Mn^{2+}. The compositions of the samples will be labeled by indicating only the x, y, and z proportions of activators.

The samples were prepared using La_2O_3 (Johnson Matthey 99.99%), CeO_2, Tb_4O_7, and As_2O_3 (Cerac 99.99%), MgO (Cerac 99.6%), $MnCO_3$ (Cerac 99.5%), and B_2O_3 (Cerac 99.9%). The dry starting materials were carefully mixed, introduced into a vitreous carbon crucible, and decarbonated at 500°C. Then the temperature was progressively raised to 1300°C and held for 1 h at this value. The melts were cooled under a continuous nitrogen flow, at the rate of 16°/min down to 700°C and at 25°/min to the room temperature. The molten glasses were annealed at 600°C for 5 h and cooled down to room temperature at 0.5°/min.

Actually the proportions of starting materials were chosen to take account of various losses occurring by evaporation during the elaboration process. The sample compositions were checked by chemical analysis after dissolution

0022-4596/96 $18.00

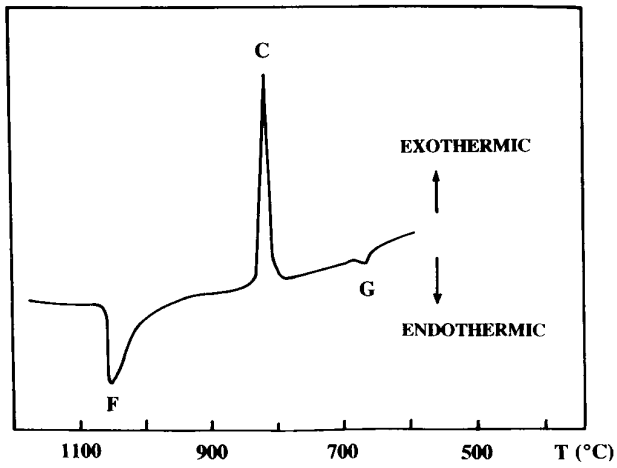

FIG. 1. DTA curve for glassy $LaMgB_5O_{10}$.

in concentrated perchloric acid. The proportions of magnesium and rare earth were determined by complexometric titration, and the rate of manganese and boron, respectively, by atomic absorption and pH titration.

As an example Fig. 1 gives the DTA curve for a glass of composition $LaMgB_5O_{10}$. The sample was heated at a rate of 350°C/h. The temperatures of the vitreous transition, crystallization and melting are, respectively, 660, 830, and 1050°C. The X-ray pattern of the product of recrystallization is strictly identical to that of the crystalline phase. The glass density (3.38) is slightly lower than that of the crystal (3.87). The refraction index measured at $\lambda = 633$ nm is 1.65.

II.2. Spectroscopic Measurements

The ^{11}B NMR spectra were recorded using a MLS 200 BRUKER spectrometer working in conjunction with a superconducting magnet (4.75 T) at 64.168 MHz and using the quadrupole echo (QECHO) program (pulse program, 90°; pulse length, 3 μs; recycle time, 30 s).

The emission spectral distribution was analyzed with a JOBIN-YVON HRS3 monochromator and detected using a R928 HAMAMATSU photomultiplier. The excitation source was a high pressure xenon lamp emitting between 200 and 1000 nm. The fluorescence decays have been recorded under the pulsed excitation of a 803 A SOPRA nitrogen laser emitting 8 ns pulses at 337 m. The signals were detected with a RTC 56DUVP photomultiplier mounted on a JOBIN-YVON HRS 640 monochromator and connected to a PAR M 162/165 boxcar averager.

The quantum efficiencies of the Mn^{2+} and Ce^{3+} luminescences have been measured on powders, the particle size of which being lower than 40 μm, by comparison with the characteristics of, respectively, Zn_2SiO_4:Mn (NBS 1028) and $CaWO_4$:Pb(NBS 1026) standards.

III. INVESTIGATION BY NMR SPECTROSCOPY AND MAGNETIC MEASUREMENTS

III.1. Structural Investigation by NMR Spectroscopy

The crystal structure of $LaMgB_5O_{10}$ was solved by Saubat *et al.* (4). Two-dimensional layers of B_5O_{10} composition are linked together by the magnesium and lanthanum ions. The boron–oxygen unit contains three BO_4 tetrahedra and two BO_3 triangles sharing common corners. The magnesium atoms are located in strongly distorted oxygenated octahedra sharing common edge to form a kind of pair ($d_{Mg-Mg} = 3.22$ Å). The lanthanum ions are surrounded by ten oxygens.

The stereochemistry of borates can be investigated by NMR spectroscopy in order to determine the respective numbers of trigonal BO_3 and tetrahedral BO_4 groups. The NMR signals of both crystalline and vitreous $LaMgB_5O_{10}$ are compared in Fig. 2. The fraction N_4 of tetracoordinated boron atoms and the quadrupole coupling constant of the trigonal BO_3 groups were calculated by using a computing simulation procedure given by Taylor *et al.* (5).

In both crystalline and vitreous forms, the N_4 value is 0.59 ± 0.04, which is consistent with the value deduced from the crystal structure ($N_4 = 0.6$) and consequently glass and crystal can be assumed to have almost identical boron–oxygen network. The ^{11}B quadrupole coupling constant e^2qQ calculated from the BO_3 component is 2.53 MHz, which is in good agreement with values previously reported for crystals and glasses containing trigonal and tetrahedral groups (6). However it is lower than those found for materials containing only the BO_3 entity. For instance in $LaBO_3$, the crystal structure of which contains discrete BO_3 triangles, e^2qQ is equal to 2.74 MHz (6). A

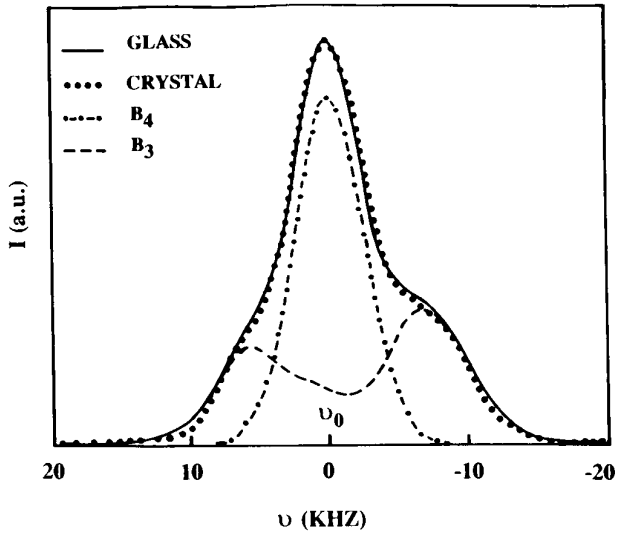

FIG. 2. ^{11}B NMR spectra for crystalline and vitreous $LaMgB_5O_{10}$ (B_4 and B_3 are the simulated components of respectively BO_4 and BO_3 units).

TABLE 1

Comparison between Experimental and Theoretical Curie Constants in the Case of Cerium or Manganese Single Doped Glasses

		$C_{exp.}$	$C_{theor.}$
Cerium glasses	$x = 5$	0.77 ± 0.05	0.81
	$x = 11.5$	0.77 ± 0.05	0.81
Manganese glasses	$z = 1$	4.22 ± 0.08	4.37
	$z = 25$	4.24 ± 0.08	4.37

close value (2.76 MHz) is also found for the boroxol cycle in the pure B_2O_3 glass (7). A relative low value for this parameter could be related to an increase of the ionic character of the boron–oxygen bond, but such an interpretation is still controverted.

III.2. Magnetic Properties of Glasses Containing Cerium and Manganese

The magnetic susceptibilities χ of several glasses have been measured between 4.2 and 300 K. The plotting of χ^{-1} vs T results in a straight line at high temperature. Table 1 collects the corresponding experimental results.

For the samples containing only Ce^{3+}, a deviation from the Curie law is detected at low temperature. It is related to the influence of the crystal field which perturbs the levels of ions by much more than kT, the ground state $J = 5/2$ being splitted into three Kramers doublets.

For the samples containing only Mn^{2+}, (i) at low concentration a Curie law is observed in the whole range of temperature and (ii) at high concentration a deviation from the straight line at low temperature reflects the appearance of an antiferromagnetic ordering with a low Neel temperature ($T_N < 4.2$ K).

In addition the experimental Curie constants of codoped glasses (Ce + Mn) are close to the sum of the values obtained for single doped samples containing the same quantity of each activator. Figure 3 compares the thermal variation of the reciprocal susceptibility for the glass ($x = 5$, $z = 1$) with the curve deduced from the addition of the magnetic susceptibilities of the single doped samples ($x = 5$) and ($z = 1$).

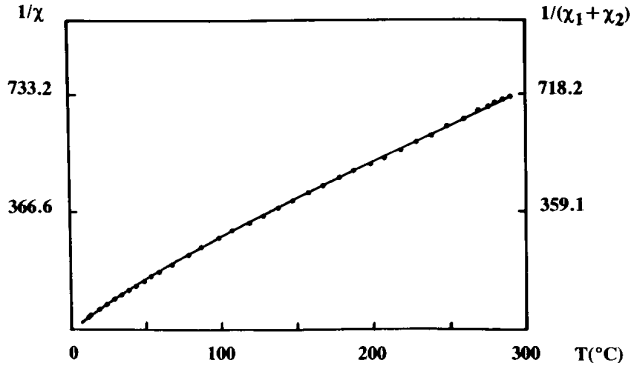

FIG. 3. Comparison between the thermal variation of the reciprocal susceptibility χ for the codoped glass ($x = 5$, $z = 1$) (· ·) with the curve (—) deduced from the addition of the magnetic susceptibilities χ_1 and χ_2 of the single doped samples ($x = 5$) and ($z = 1$).

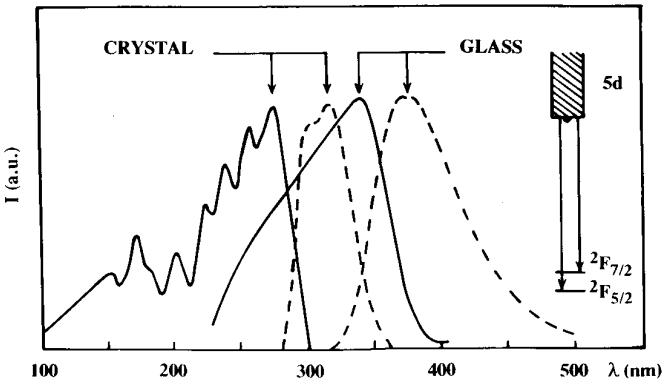

FIG. 4. Comparison between excitation (—) and emission (--) spectra of vitreous (this work, $x = 1.25$) and crystalline (8) forms of $La_{0.90}Ce_{0.10}MgB_5O_{10}$.

IV. LUMINESCENCE PROPERTIES OF SINGLE DOPED GLASSES

IV.1. The Luminescence of Cerium Glasses

(*i*) *Comparison between vitreous and crystalline materials.* Figure 4 compares the excitation and emission spectra of both forms of $LaMgB_5O_{10}:Ce^{3+}$. The $4f \leftrightarrow 5d$ bands are markedly red shifted in the vitreous material. This evolution is related to the creation of multisites for Ce^{3+}. However the close low Stokes shifts (4500 cm^{-1} for the crystal and 3100 cm^{-1} for the glass) are determined by the rigidity of the similar boron–oxygen networks.

Incidentally the resulting overlapping between excitation and emission spectra leads to a potential significant reabsorption of the high energy emitted photons and accordingly to a red shift of the light emitted by a block in comparison with that emitted by powder glasses of same composition.

(*ii*) *Existence of two Ce^{3+} centers in the glasses.* Usually in glasses the activators are distributed over a continuum of sites. Figure 5 shows typical evolution of the emission spectrum of the $x = 0.1$ glass as a function of the excitation wavelength, respectively 254 and 340 nm. Two distinct bands can be detected. The first one (A) peaking at 27,770 cm^{-1} ($\lambda \simeq 350$ nm) is observed only under a higher energy excitation ($\lambda < 333$ nm). The second band (B) peaking at 25,000 cm^{-1} ($\lambda \simeq 400$ nm) is observed under a lower energy excitation. In a parallel way the low energy side of the

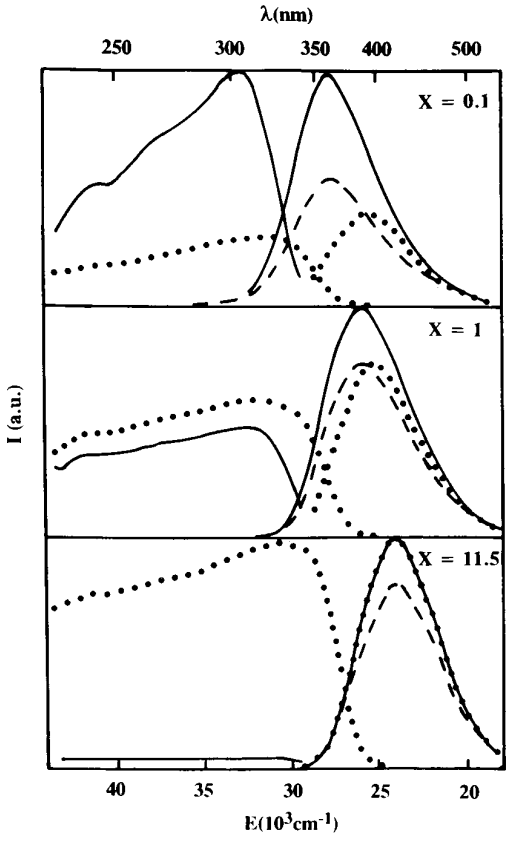

FIG. 5. Evolution at room temperature of Ce^{3+} excitation and emission spectral distributions as a function of recording conditions, for various single doped glasses ($x = 0.1$, 1, and 11.5): excitation spectra for the 350 (—) or 430 nm (• •) emission; emission spectra under a 254 (--), 300 (—), or 340 nm (• • •) excitation.

excitation band is red shifted by recording the excitation spectrum for the 340 nm emission and then for the 430 nm one. These experiments evidence the existence of Ce^{3+} fluorescent centers respectively at high energy (A) and at low energy (B).

As the cerium concentration increases, the (A) band is progressively red shifted whereas (B) remains well localized at the same energy. This evolution is exemplified in Fig. 6 which compares the spectral distributions of Ce^{3+} emission for the $x = 0.1$, $x = 1$, and $x = 11.5$ glasses, under the same 270 nm excitation beam, i.e., under the conditions where the (A) and (B) emitters are simultaneously excited. For a relatively low cerium concentration the emission band can be divided into its (A) and (B) parts. In contrast the richest cerium glass exhibits only the (B) emission due to the fast energy transfer from the high energy to the low energy centers.

(*iii*) *Emission decays.* The decays of the cerium emission were recorded at 370 and 430 nm under a 337 nm excitation for various cerium concentrations. Since the curves were not a single exponential, a mean decay constant τ_m was defined as

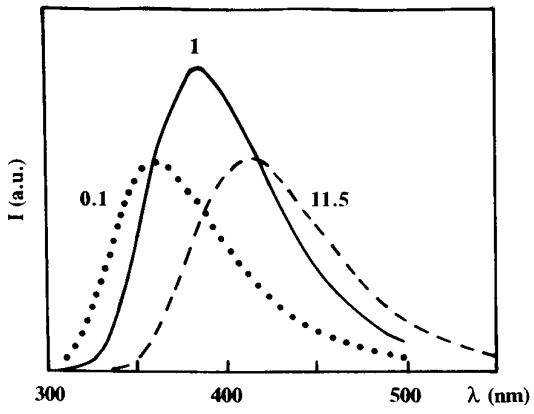

FIG. 6. Evolution of Ce^{3+} emission spectrum as a function of cerium concentration ($x = 0.1$, 1, and 11.5; $\lambda_{exc.} = 270$ nm; $T = 300$ K).

$$\tau_m = \frac{\int_0^\infty I(t)t\,dt}{\int_0^\infty I(t)\,dt} \qquad [1]$$

The values measured at 370 nm ($\tau_m = 33$ ns) and at 430 nm ($\tau_m = 37$ ns) are very close and roughly independent of the cerium concentration since in the experimental conditions the (B) emitters are preferentially excited.

(*iv*) *Quantum efficiency vs Ce^{3+} concentration.* Under a 270 nm excitation, as the activator concentration increases, the quantum efficiency η exhibits a maximum for the composition $x = 1$ ($\eta = 0.6$). Its value remains high (0.45) even for the richest cerium glasses in spite of a weak concentration quenching of the emission intensity (Fig. 7).

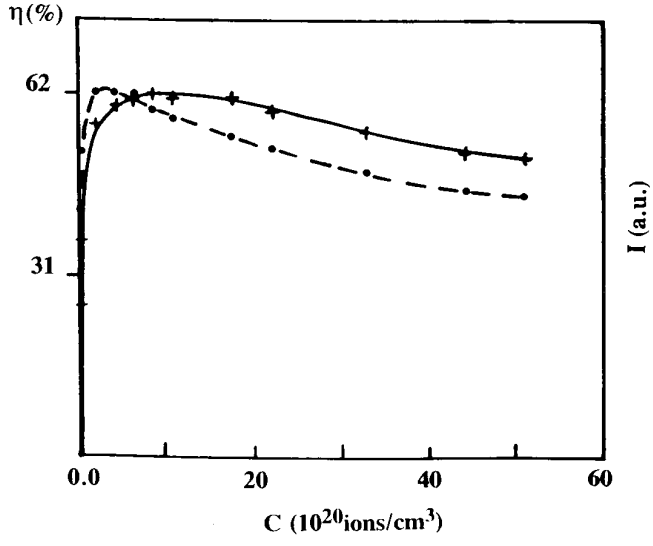

FIG. 7. Ce^{3+} emission intensity (–+–) and quantum efficiency (-• -•) vs cerium concentration for single doped glasses ($\lambda_{exc.} = 270$ nm, $T = 300$ K).

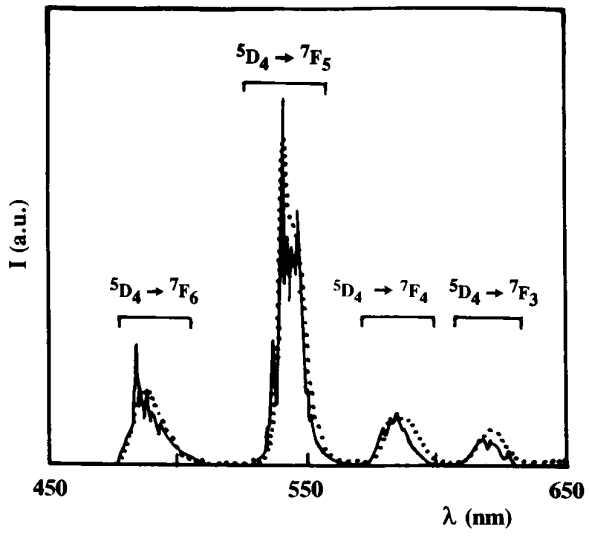

FIG. 8. Superposition of the spectral distributions of Tb^{3+} emission for the glass ($y = 7$) (• •) and for the crystalline compound with same composition (—) ($\lambda_{exc.} = 254$ nm, $T = 300$ K).

In conclusion, the results can be interpreted through a model involving two types of Ce^{3+} centers: regular centers (A) and anomalous centers (B) affected by the presence of a neighboring trap of undefinite origin.

Nevertheless it is not allowed to estimate the respective (A) and (B) emission probabilities in absence of decay measurements under a higher energy excitation. The concentration variation of the quantum efficiency can be explained by the combination of two factors: a high probability of the energy transfer from (A) to (B) but also a migration of this energy among the (A) center subnetwork.

IV.2. The Luminescence of Terbium Glasses

Figure 8 compares the Tb^{3+} emission spectra of the glass ($y = 7$) and of the crystal of identical composition under a 254 nm excitation. The observed bands originate from the $^5D_4$ level with the usual $^5D_4 \rightarrow {}^7F_5$ intense green emission. The fair coincidence between the two curves is a consequence of the $4f \rightarrow 4f$ character of the involved transitions.

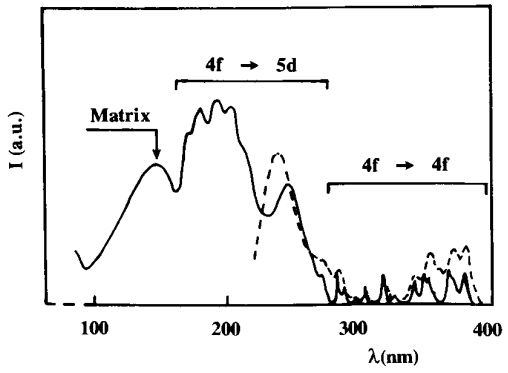

FIG. 9. Comparison between the Tb^{3+} excitation spectra for the 540 nm emission for the glass ($y = 7$) (--) and for the crystalline compound of same composition (—) at $T = 300$ K.

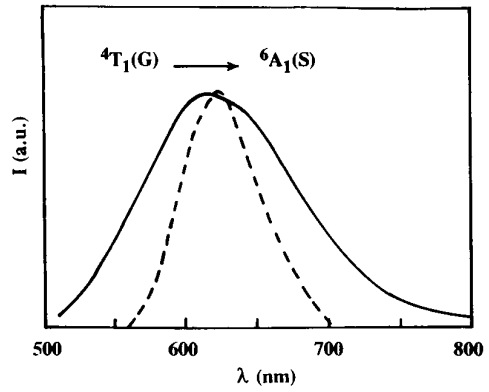

FIG. 10. Mn^{2+} emission for the glass ($z = 1$) (—) and the crystalline material of same composition (--) under a 415 nm excitation, at $T = 300$ K.

The corresponding excitation spectra for the $^5D_4 \rightarrow {}^7F_5$ emission are given in Fig. 9. At higher energy, the intense band corresponds to the parity-allowed $4f \rightarrow 5d$ transitions. At lower energy are found the weak intensity lines resulting from the forbidden transitions between levels of the $4f^8$ configuration.

IV.3. The Luminescence of Manganese Glasses

The spectral distributions of Mn^{2+} emission for the glass and the crystal of composition ($z = 1$) are given in Fig. 10. The red fluorescence is provided by manganous ions in octahedral sites. The distribution of these ions in the multisites of the glass broadens the emission band. A modification of the excitation wavelength has no influence on the spectral distribution of this emission but an increase of the manganese concentration red shifts the emission maximum.

The fluorescence mechanism involves both Laporte and spin forbidden transitions so that the intensity of the $^4T_1(G) \rightarrow {}^6A_1$ emission is weak. In contrast the quantum efficiency η is very high when the amount of manganese is low, e.g., $\eta = 0.97$ for a ($z = 3$) glass. Figure 11 represents the variation of η vs Mn^{2+} concentration, measured under a 410 nm excitation. This curve shows a more efficient concentration quenching than that observed for Ce^{3+} emission.

The excitation spectrum of Mn^{2+} for the ($z = 1$) glass is given in Fig. 12. Its profile is independent of the emission wavelength and of the activator concentration. The various bands have been identified from the Tanabe–Sugano energy level diagram for a d^5 configuration. The crystal field strength Δ and the Racah parameters B and C have been calculated with the weak field matrices of the quartet levels given by Bingham and Parke (9). A least square fitting

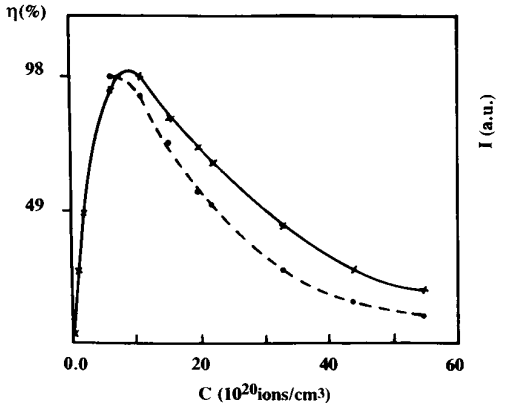

FIG. 11. Mn^{2+} emission intensity (xx) and quantum efficiency (•---•) vs manganese concentration for single doped glasses ($\lambda_{exc.} = 415$ nm and $T = 300$ K).

(Table 2) leads to $\Delta = 6800\ cm^{-1}$, $B = 619\ cm^{-1}$, and $C = 3562\ cm^{-1}$. These results agree with the data of previous investigations (1, 10, 11) and are consistent with the location of Mn^{2+} in octahedral sites.

V. SENSITIZATION OF Tb^{3+} AND Mn^{2+} LUMINESCENCE BY Ce^{3+} IN CODOPED GLASSES

Ce^{3+} sensitizes efficiently Tb^{3+} and Mn^{2+} emissions under UV excitation. The luminescence of Mn^{2+} is strongly enhanced: for example the Mn^{2+} emission is 10 times as much intense in the glass ($x = 1$, $z = 1$) than that in the glass

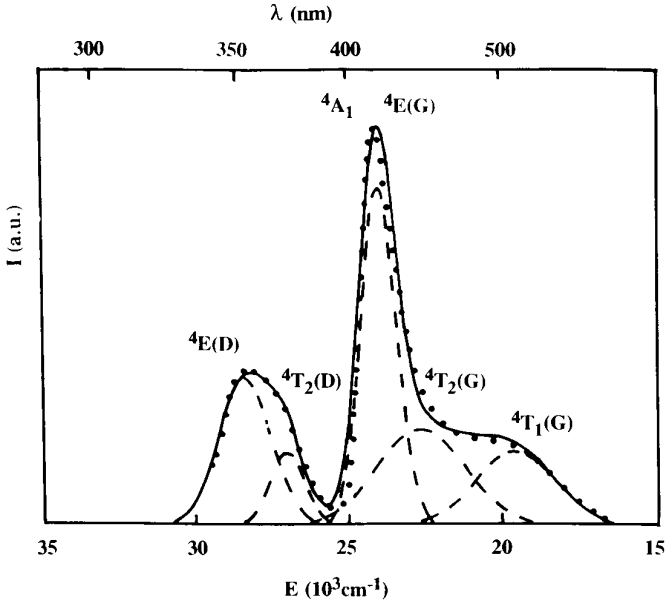

FIG. 12. Excitation spectrum of Mn^{2+} for the ($z = 1$) manganese single doped glass (• •) ($\lambda_{em.} = 620$ nm, $T = 300$ K). (--) deconvolution of the experimental spectrum, (—) simulated spectrum.

TABLE 2
Mn^{2+} Excitation Bands for a $LaMgB_5O_{10}:Mn^{2+}$ Single Doped Glass; Calculated and Observed Positions

Excited level	Calculated position	Observed position
$^4T_1(^4G)$	508 nm	508 ± 2 nm
	19,669 cm^{-1}	19,667 ± 50 cm^{-1}
$^4T_2(^4G)$	448 nm	441 ± 8 nm
	22,330 cm^{-1}	22,667 ± 400 cm^{-1}
$^4A_1$, $^4E(^4G)$	417 nm	417 ± 1 nm
	24,000 cm^{-1}	24,000 ± 50 cm^{-1}
$^4T_2(^4D)$	372 nm	370 ± 2 nm
	26,905 cm^{-1}	27,000 ± 100 cm^{-1}
$^4E(^4D)$	353 nm	353 ± 1 nm
	28,333 cm^{-1}	28,333 ± 50 cm^{-1}

($z = 1$). Such sensitization requires a good overlapping between the Ce^{3+} emission and the Mn^{2+} (or Tb^{3+}) excitation spectra. This condition is completely fullfilled in both cases (Fig. 13). Accordingly the intense band characterizing the $4f \rightarrow 5d$ Ce^{3+} transitions appears in the excitation spectrum recorded for the $Tb^{3+}(^5D_4 \rightarrow {}^7F_5)$ or Mn^{2+} ($^4T_1 \rightarrow {}^6A_1$) emissions.

The mechanism of sensitization of terbium luminescence by cerium has been investigated in several systems. Usually the interaction between Ce^{3+} and Tb^{3+} is of electric dipole–dipole nature for relatively low acceptor concentrations.

In contrast, the nature of the Ce^{3+}–Mn^{2+} coupling is still discussed.

The existence of a radiative process can be ruled out since the spectral distribution of the Ce^{3+} emission in presence or in absence of Mn^{2+} is identical, even in the range of Mn^{2+} excitation.

Therefore, for the cerium–manganese codoped glasses, the experimental parameters were analyzed in the context of the theories describing the electric dipole–dipole interaction or the exchange effect. The investigated glasses contained a very low proportion of donors ($x = 0.1$) to avoid Ce^{3+}–Ce^{3+} interactions. The simultaneous emissions of Ce^{3+} and Mn^{2+}, the Ce^{3+} emission quantum yield and decay were measured for increasing proportion of manganese. The decay constant value was found to be independent of the emission wavelength selected for the decay recording.

V.1. Theoretical Aspect

(*i*) *Basic formalism for energy transfer through a direct interaction between electric dipoles.* For an energy transfer between electric dipoles, the transfer probability is proportional to R^{-6} where R is the donor–acceptor distance. The time dependence of the donor emission decay, following Inokuti and Hirayama (12), is given by

$$I(t) = I_0 \exp(-t/\tau_0 - \sqrt{\pi}c/c_0\sqrt{t/\tau_0}). \qquad [2]$$

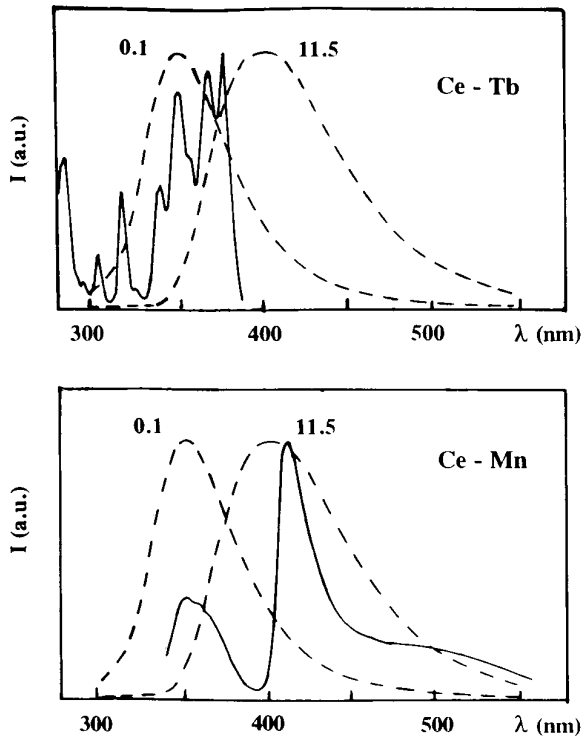

FIG. 13. Overlapping between the emission spectrum of Ce^{3+} ($\lambda_{exc.} = 270$ nm) (--) and the excitation bands of Tb^{3+} (for $\lambda_{em.} = 540$ nm) and Mn^{2+} (for $\lambda_{em.} = 620$ nm), at $T = 300$ K (—). Samples used for the various recordings: ($x = 0.1$) and ($x = 11.5$) glasses for Ce^{3+} emission, ($y = 7$) glass for Tb^{3+} excitation, and ($z = 1$) glass for Mn^{2+} excitation.

c is the acceptor concentration; c_0 is the critical concentration for which the donor → acceptor transfer probability P_{da} is equal to $1/\tau_0$, if τ_0 is the donor excited state lifetime in absence of acceptor.

The relative quantum yield of donor luminescence, i.e., the ratio of the luminescence yields in the presence(η) and the absence (η_0) of the acceptor, is given by

$$\eta/\eta_0 = 1/\tau_0 \int_0^\infty I(t)\, dt. \qquad [3]$$

For the dipole–dipole transfer, Forster (13) derived the formula

$$\eta/\eta_0 = 1 - \sqrt{\pi} x \exp(x^2)\,[1 - \mathrm{erf}(x)], \qquad [4]$$

where $x = 1/2\sqrt{\pi}\, c/c_0$.

(*ii*) *Basic formalism of energy transfer by exchange mechanism.* The influence of energy transfer by exchange mechanism on the donor emission has been discussed by Dexter (14) and by Inokuti and Hirayama (12).

The probability P_{da} of a transfer between a donor and an acceptor is given by

$$P_{da} = 2\pi/\hbar Z^2 \int f_d(E) F_a(E)\, dE, \qquad [5]$$

where $Z^2 = K^2 \exp(-2\,R/L)$ in which K is a constant with a dimension of energy, L is the effective average Bohr radius, R is the donor–acceptor distance, and $f_d(E)$ and $F_a(E)$ represent the normalized spectral distribution functions of the donor emission and the acceptor excitation. The time evolution of the donor emission intensity is given by

$$I(t) = I_0 \exp\left(-t/\tau_0 - \frac{c}{c_0 \gamma^3}\, g(z)\right), \qquad [6]$$

where $z = t/\tau_0 \exp \gamma$, $g(z)$ is the Taylor series expansion

$$g(z) = 6z \sum_{m=0}^{\infty} \frac{(-z)^m}{m!(m+1)^4}, \qquad [7]$$

c is the acceptor concentration and the critical concentration c_0 can be written

$$c_0 = \frac{3}{4\pi R_0^3},$$

where R_0 is the donor–acceptor distance for which $P_{da} = 1/\tau_0$, and finally

$$\gamma = \frac{2R_0}{L}. \qquad [8]$$

In the case of exchange interaction the donor luminescence yield follows the Perrin law

$$\eta/\eta_0 = \exp(-\alpha c), \qquad [9]$$

where α is a positive constant.

V.2. Experimental Investigation of the $Ce^{3+} \rightarrow Mn^{2+}$ Energy Transfer Mechanism

The experimental data were analyzed in the double context of the above theories, according to the procedure described by Inokuti (12) and adopted for instance by Soules *et al.* in the case of the $Sb^{3+} \rightarrow Mn^{2+}$ energy transfer in fluorophosphate phosphors (15).

It was not possible to distinguish the own contribution of the (A) or (B) donors (see Section IV.1(ii)). The quantum yields of Ce^{3+} luminescence were measured for $x = 0.1$ under a 270 nm excitation whereas the decays of the Ce^{3+} emission were recorded at 370 and 430 nm under a 337 nm excitation. Actually, since the decay curves are independent of the wavelength emission, it was assumed that both (A) and (B) centers were probed under our experimental conditions.

The cerium emission decay curves are nonexponential and this characteristic is more marked as the acceptor

TABLE 3
Experimental Data for the $Ce^{3+} \rightarrow Mn^{2+}$ Energy Transfer Mechanism Investigation

Z	$C(10^{20}$ ions $Mn^{2+}/cm^3)^a$	$d \pm 0.04^b$	$(a \pm 2)\%^c$	$\eta(\%)^d$	η/η_0	$(\tau_m \pm 2)$ns^e	τ_m/τ_0
0	0	3.39	52	53 ± 2	1.000	36	1.00
0.1	0.22 ± 0.01	3.39	52	51 ± 2	0.960	36	1.00
0.5	1.10 ± 0.02	3.39	54	44 ± 2	0.840	35	0.98
1	2.19 ± 0.03	3.40	59	39 ± 2	0.740	34	0.96
3	6.57 ± 0.07	3.42	59	17 ± 1	0.320	32	0.88
5	11.0 ± 0.2	3.44	61	8.5 ± 0.4	0.170	30	0.84
7	15.3 ± 0.2	3.46	59	6.3 ± 0.3	0.120	28	0.80
9	19.7 ± 0.3	3.49	56	3.0 ± 0.2	0.057	27	0.75
10	21.9 ± 0.3	3.50	56	2.4 ± 0.2	0.045	26	0.72
15	32.9 ± 0.4	3.55	56	0.6 ± 0.1	0.011	23	0.66
20	43.6 ± 0.5	3.60	56			20	0.56
25	54.7 ± 0.6	3.66	56			18	0.50

Note. $T = 300$ K, (0.1 Ce_2O_3, zMnO) glasses.
[a] Manganese (+II) concentration.
[b] Density.
[c] Absorption percentage at 270 nm.
[d] Quantum efficiency of Ce^{3+} luminescence under a 270 nm excitation.
[e] Time decay constants of Ce^{3+} emission under a pulsed excitation at 337 nm.

concentration increases. Therefore the mean time constant τ_m given by [1] was introduced to interpret quantitatively the experimental values. All the relevant data are listed in Table 3 and have been examined with the steps described below.

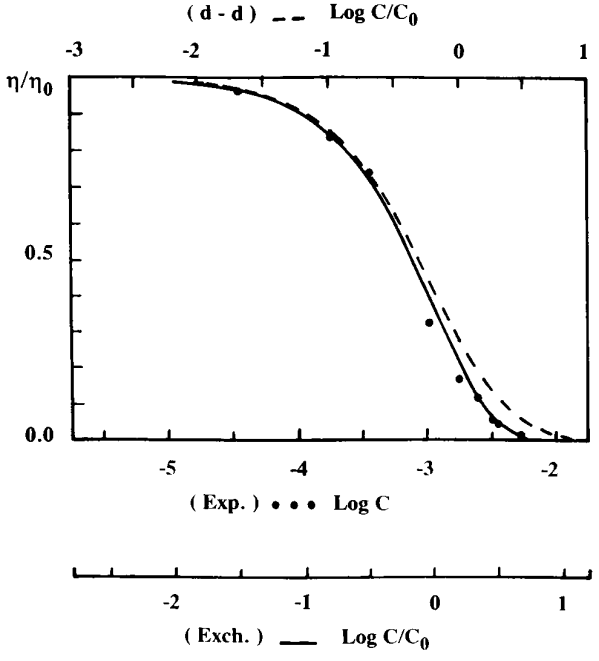

FIG. 14. Fitting of the experimental variations of η/η_0 vs log C (• •), in the hypothesis of an electric dipolar interaction (--) or of an exchange interaction (—), for the ($x = 0.1$, z) glasses.

Assuming an electric dipole–dipole interaction, the best fit of the experimental variations of η/η_0 vs c, using [4], is obtained for $c_0 = 1.78 \times 10^{-3}$ mole cm^{-3} ($C_0 \simeq 2.9 \times 10^{21}$ ions cm^{-3}, $z \simeq 13$), i.e., $R_0 = 5.98$ Å. In this hypothesis, the theoretical decays presented in Fig. 15 were obtained through Eq. [2], with $\tau_0 = 36$ ns.

In the context of an exchange interaction mechanism, the comparison of the experimental $\eta/\eta_0 = f(\tau_m/\tau_0)$ variations with the corresponding theoretical curves proposed in (12) leads to $\gamma = 30$. The best fit of $\eta/\eta_0 = f(\log c)$, for $\gamma = 30$, by using the numerical tables $\eta/\eta_0 = f(\log c/c_0)$ (12) results then in $c_0 = 1.12 \times 10^{-3}$ mole cm^{-3} ($C_0 \simeq 6.7 \times 10^{20}$ ions cm^{-3}, $z \simeq 3$), i.e., $R_0 = 6.92$ Å. In this second hypothesis, the theoretical decays presented in Fig. 15 were obtained through Eq. [6], with $\tau_0 = 36$ ns.

The relative quantum yields η/η_0 calculated for both models are compared in Fig. 14 to the experimental values. The influence of the exchange interaction is progressively evidenced for higher concentrations of acceptor.

This tendency is strongly confirmed by calculating the theoretical Ce^{3+} luminescence decay curves for various manganese concentrations (Fig. 15): the fit with the experimental data is unambiguously better when using an exchange interaction model.

For the lowest acceptor concentrations it cannot be concluded which of the dipole–dipole or exchange mechanisms prevails, but as far as the acceptor concentration increases, the predominant effect of exchange is clearly evidenced.

Due to the close relationship between the atomic arrangement existing in the studied glasses and the structure

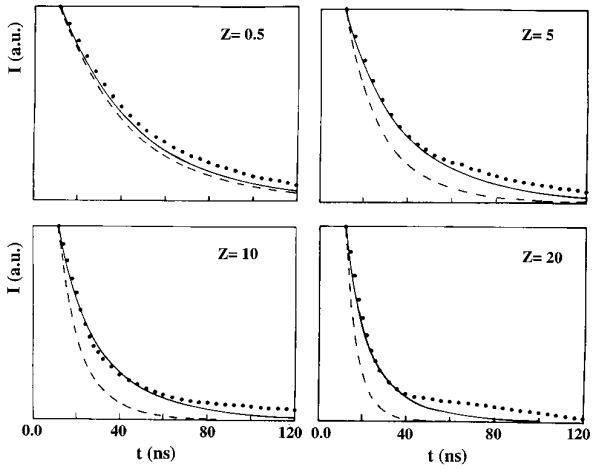

FIG. 15. Fitting of the experimental decay curves of Ce^{3+} luminescence (• •) for the cerium–manganese codoped glasses with $x = 0.1$ and various z values, in the hypothesis of an electric dipolar interaction (--) or of an exchange interaction (—).

TABLE 4

Characteristics of the Emissions, under a 254 nm Excitation, of Some Glasses Simultaneously Activated by Ce^{3+}, Tb^{3+}, and Mn^{2+}, in Comparison with That of the Standard Halophosphate $Ca_5(PO_4)_3(F, Cl):Sb^{3+}$, Mn^{2+} ($T = 300$ K)

Sample label	Composition	Chromaticity coordinates X_t	Y_t	Z_t	I_g/I_h[a]
1	$0.5Ce_2O_3$; $0.2Tb_2O_3$; 0.2MnO	0.27	0.28	0.45	0.5
2	$1Ce_2O_3$; $0.5Tb_2O_3$; 0.5MnO	0.33	0.38	0.29	0.4
3	$5Ce_2O_3$; $2Tb_2O_3$; 1MnO	0.39	0.47	0.14	0.6
4	$3Ce_2O_3$; $2Tb_2O_3$; 1MnO	0.38	0.47	0.15	0.6
5	$3Ce_2O_3$; $2Tb_2O_3$; 0.5MnO	0.36	0.50	0.14	0.7
H	$Ca_5(PO_4)_3(F, Cl):Sb^{3+}$, Mn^{2+}	0.40	0.41	0.19	1

[a] I_g, integrated surface of the glass emission; I_h, integrated surface of the halophosphate emission.

of the crystalline borates of same composition, the shortest Ce–Mn distance is approximately 3.80 Å. Consequently the exchange mechanism may involve a direct overlapping of the donor and acceptor orbitals but more probably needs an intermediate oxygen like in superexchange interaction. The probability of the existence of such coupled (Ce–Mn) entities increases with the acceptor concentration.

VI. THE LUMINESCENCE OF GLASSES SIMULTANEOUSLY ACTIVATED BY Ce^{3+}, Tb^{3+}, AND Mn^{2+}

The glasses activated by Ce^{3+}, Tb^{3+}, and Mn^{2+} exhibit simultaneously the blue cerium emission, the green terbium emission, and the red manganese emission under a 254 nm excitation, i.e., using a low mercury vapor lamp as an excitation source (Fig. 16).

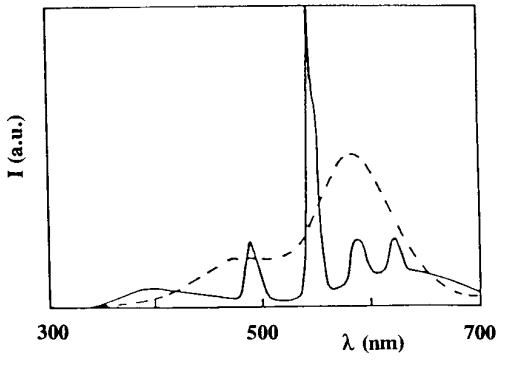

FIG. 16. Comparison at 300 K, under the same 254 nm excitation, between the emission spectrum of the standard halophosphate $Ca_5(PO_4)_3$ (F, Cl): Sb^{3+}, Mn^{2+} (--) and that of the ($x = 5$, $y = 2$, $z = 1$) ground glass (—).

The combination of these emissions provides white or greenish-yellow light. The Ce^{3+} ions acts both as the blue emitter and as a sensitizer for the Tb^{3+} and Mn^{2+} ions.

The global emission was characterized by its chromaticity coordinates in the C.I.E. chromaticity diagram and by comparing its whole emission intensity with that of the standard calcium halophosphate $Ca_5(PO_4)_3$ (F, Cl):Sb^{3+}, Mn^{2+} under the same experimental conditions. Both factors—chromaticity and intensity—vary by changing the activator concentrations. Some examples are listed in Table 4 and the corresponding representative points are reported on the chromaticity diagram (Fig. 17). The intensity of the emitted light is approximately 60% that of the standard, and the color of the emission can be largely modified by changing the respective rates of the activators.

VII. CONCLUSION

Glasses of composition $LaMgB_5O_{10}$ activated with only cerium (III), with cerium (III) and terbium (III), or with cerium (III), terbium (III), and manganese (II) can be easily prepared. This borate medium allows a good chemical compatibility between these ions. From the structural viewpoint, the NMR study concludes to the similarity between the boron–oxygen network in glasses and crystals. Mn^{2+} ions are located in octahedral sites. However the paramagnetism of the rich manganese glasses can be interpreted as the result of a decoupling of the pair of octahedral sites existing in the crystallized phase structure; otherwise a high magnetic ordering temperature would be observed. For comparison, the Neel temperature of MnO ($d_{Mn-Mn} = 4.43$ Å) is 115 K (16).

Ce^{3+} ions are located in a continuum of sites (A) but

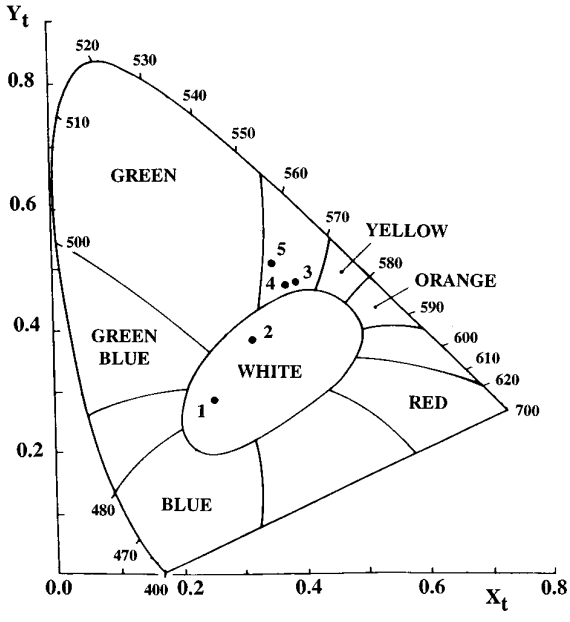

FIG. 17. Representative points on the chromaticity diagram of the emission of some selected glasses coactivated by Ce^{3+}, Tb^{3+}, and Mn^{2+}. The correspondence between the label of every sample (1, 2, 3, 4, or 5) and its composition is given in Table 4.

the emission of trap centers (B) is always detected and becomes unique for the cerium rich glasses due to an energy migration from (A) to (B).

Sensitization of terbium and manganese by cerium allows a simultaneous emission of these three ions under UV excitation. In these glassy materials the investigation of the cerium–manganese energy transfer is rather complex but was tentatively examined in the context of possible interaction through electric dipoles or exchange mechanism. Since the cerium emission decay is never exponential, the analysis of the decay curves requires the introduction of a mean constant time. Within this approximation the evolution of the cerium emission vs manganese concentration cannot be explained only on the basis of electric dipole interaction and the involvement of the exchange mechanism allows the beginning of the decay curves to be fitted, i.e., in the temporal part excluding the influence of the trap centers.

Finally the possibility of white light emission by this complex system is demonstrated. The intensity is lower than that of the standard calcium halophosphate measured under the same conditions. But actually the main purpose of this study was a fundamental approach of the involved fluorescence processes and no optimization of the luminescence quantum yield was attempted in this first step. Several parameters, particularly the base glass composition and the respective activator concentration, can be modified to increase the efficiency of these luminophors.

REFERENCES

1. J. C. Zhang, C. Parent, G. Le Flem, and P. Hagenmuller, *J. Solid State Chem.* **93,** 17 (1991).
2. J. Th. W. De Hair and J. T. C. Van Kemenade, "Paper 54 presented at the 3rd International Symposium on Science and Technology of Light Sources. Toulouse, France, April 18–21, 1983."
3. B. Looye, J. Th. W. De Hair, and C. Bakker, European Patent, NL 7905680 (23.07.79).
4. B. Saubat, M. Vlasse, and C. Fouassier, *J. Solid State Chem.* **34,** 271 (1980).
5. P. C. Taylor and P. J. Bray, *J. Magn. Res.* **2,** 305 (1970).
6. P. J. Bray, J. O. Edwards, J. G. O'Keefe, V. F. Ross, and I. Tatsukaki, *J. Chem. Phys.* **35,** 435 (1961).
7. A. H. Silver and P. J. Bray, *J. Chem. Phys.* **29,** 984 (1958).
8. B. Saubat, C. Fouassier, and P. Hagenmuller, *Mater. Res. Bull.* **16,** 193 (1981).
9. K. Bingham and S. Parke, *Phys. Chem. Glasses* **6(6),** 224 (1965).
10. P. E. Menassa, D. J. Simkin, and P. Taylor, *J. Luminesc.* **35,** 223 (1986).
11. L. N. Feuerhelm, S. M. Sibley, and W. A. Sibley, *J. Solid State Chem.* **54,** 164 (1984).
12. M. Inokuti and F. Hirayama, *J. Chem. Phys.* **43,** 1978 (1965).
13. Th. Forster, *Radiat. Res. Suppl.* **2,** 326 (1960).
14. D. L. Dexter, *J. Chem. Phys.* **21,** 836 (1953).
15. T. F. Soules, R. L. Bateman, R. A. Hewes, and E. R. Kreidler, *Phys. Rev. B* **7(4),** 1657 (1972).
16. D. H. Martin, "Magnetism in Solids." Iliffe Book Ltd. London, 1967.